

## Article

# Effect of Thermochemical Boronizing of Alumina Surface on the Borate Crystals Growth and Interaction with Nickel and Nickel Alloy

Jelena Škamat <sup>1,\*</sup>, Aleksandr Lebedev <sup>2</sup>, Olegas Černašėjus <sup>2</sup> and Rimvydas Stonys <sup>1</sup>

<sup>1</sup> Laboratory of Composite Materials, Faculty of Civil Engineering, Vilnius Gediminas Technical University, 08217 Vilnius, Lithuania

<sup>2</sup> Department of Mechanics and Materials Engineering, Faculty of Mechanics, Vilnius Gediminas Technical University, 03224 Vilnius, Lithuania

\* Correspondence: jelena.skamat@vilniustech.lt

**Abstract:** Wettability at the metal-ceramic interface is highly important for the development of modern composite materials. Poor wettability by metal melts restricts the use of alumina in protective metal matrix composite (MMC) coatings. In the present experimental study, the possibility to modify wetting properties of alumina by thermochemical surface boronizing was investigated. The results of SEM, EDS, XRD and XPS characterisation of surfaces revealed the formation of oxygen containing Al–B compounds identified as aluminium borates ( $\text{Al}_{18}\text{B}_4\text{O}_{33}$ / $\text{Al}_4\text{B}_2\text{O}_9$ ); no signs of non-oxide Al–B compounds were observed. The shape of the single splats deposited on the boronized alumina surface by the thermal spray and re-melted in the furnace revealed that significant wetting improvement by self-fluxing nickel alloy did not occur. However, the improvement of adhesion between the nickel/nickel alloy and  $\text{Al}_2\text{O}_3$  surface was obtained due to formation of an intermediate layer consisting of B, O, Al and Si between the metal and ceramic surfaces at the presence of some silicon at the modified surfaces. The presented study demonstrates that the thermochemical boronizing of alumina in amorphous boron medium is a simple method to obtain a thin aluminium borate layer consisting of oriented nano-rod-like crystals, whose growing direction is predetermined by the orientation of the alumina grains' faces at surface.

**Keywords:** alumina; ceramic; thermochemical treatment; boronizing; surface modification; aluminium borate; adhesion; SEM; EDS; XRD; XPS; thermal spray



**Citation:** Škamat, J.; Lebedev, A.; Černašėjus, O.; Stonys, R. Effect of Thermochemical Boronizing of Alumina Surface on the Borate Crystals Growth and Interaction with Nickel and Nickel Alloy. *Crystals* **2023**, *13*, 4. <https://doi.org/10.3390/cryst13010004>

Academic Editor: Yuying Wu

Received: 30 November 2022

Revised: 15 December 2022

Accepted: 17 December 2022

Published: 20 December 2022



**Copyright:** © 2022 by the authors. Licensee MDPI, Basel, Switzerland. This article is an open access article distributed under the terms and conditions of the Creative Commons Attribution (CC BY) license (<https://creativecommons.org/licenses/by/4.0/>).

## 1. Introduction

Aluminium oxide, or alumina, is a relatively inexpensive and readily obtained ceramic material [1]. Alumina ceramic possesses high hardness (up to ~17 GPa), wear resistance and compressive strength (up to ~2200 MPa), along with low density (~3.6–3.9 g/cm<sup>3</sup>), excellent resistance to corrosion and chemical stability that makes alumina valuable material for protective coatings. It was shown [2] that  $\text{Al}_2\text{O}_3$  layers can be deposited on metal substrates by thermal spray methods, and the wear resistance of the surface can be significantly improved. However, alumina, similar to other ceramic materials, is brittle, and the use of pure ceramic coatings is often limited. Metal matrix composite (MMC) coatings, in which hard ceramic particles are well incorporated in a plastic metal layer, possess much better plasticity and impact toughness. Therefore, the interest in MMC coatings has been very high for the last decades. Protective coatings based on iron, nickel and cobalt alloys with the addition of carbide (most often) ceramics have gained the most widespread attention [3–5]. Alumina ceramics possessing excellent properties are not as widely used in metal matrix composite coatings. The main reason for this is poor alumina wetting by metals' melts, which impairs coating cohesion and adhesion. The appearance of a new class of protective coatings could be expected if this barrier was overcome.

Metals' melts wet ceramics essentially by chemical bond formation [6]. Earlier investigations have shown very poor alumina wettability by the melts of different metals: 134–160° contact angles were established for Cu; 122–128° for Ni; 110–130° for Fe; 114–134° for Sn; and 124° for In [6–10]. In a later investigation [11], lower contact angles were measured (83°, 84° and 95°), indicating an improvement in alumina wetting by Ni-based and Co-based superalloys with a complex alloying system—ECY768, IN738LC and CMSX486, respectively. The works mentioned above and other studies available in the field show, in general, that some improvement in wetting properties of alumina may be reached mainly by the modification of the metal melt with certain alloying elements. In the present study, an attempt was made to apply another approach—modification of the surface of aluminium oxide. In a field of metals and alloys, thermochemical treatment is known as the most effective way to modify the chemistry and property of the surface. To the best of the authors' knowledge, the enrichment of the ceramic surface with some elements by the thermochemical process has not been widely studied and presented in the literature. At the same time, according to the data available in the field, the formation of some non-oxide compounds, such as borides or borocarbides, could possibly improve the wettability conditions at the alumina-metal interface.

In the present experimental work, boron was chosen for the chemical modification of the alumina surface. There were several reasons for this. First, boron has one of the smallest atomic radii of 87 pm that makes the diffusion of boron atoms into the crystal lattice of the material of surface to be modified easier. In addition, boron is used in the self-fluxing Fe-based, Ni-based and Co-based alloys developed for thermal-sprayed coating, since boron acts as a fluxing agent (preventing the coating from oxidation), forms low-melting point eutectics together with these metals (making it easier to fuse such alloys) and participates in the formation of borides and carboborides [12]. The process of the thermochemical boronizing of steels in solid mediums is well known and widely described in the literature [13], and makes it easier to update this method for ceramics. The paper demonstrates the evolution of alumina surface morphology with increasing boronizing temperature from 800 °C to 950 °C, presents the results of surface phase analysis and gives the results of the investigation of the modified alumina surface's interaction with nickel and nickel alloy.

## 2. Materials and Methods

### 2.1. Details of the Alumina Boronizing Experiment

Alumina plates of 37 mm × 27 mm × 0.6 mm size were used for the thermochemical treatment experiments. The chemical composition of the used alumina plates was as follows: 98.6% Al<sub>2</sub>O<sub>3</sub>; 0.863% SiO<sub>2</sub>; 0.241% MgO; 0.191% CaO; 0.0628% Fe<sub>2</sub>O<sub>3</sub>; 0.0464% Na<sub>2</sub>O; and traces of P<sub>2</sub>O<sub>5</sub>, SO<sub>3</sub>, Cl, K<sub>2</sub>O, Ga<sub>2</sub>O<sub>3</sub> (in wt.%, by wavelength dispersive X-ray fluorescence spectroscopy (XRF-WD), ZSX Primus IV spectrometer (Rigaku Corp., Tokyo, Japan) with 4 kW end-window Rh anode X-ray tube; XRF analysis parameters—60 kV, 150 mA). The characteristics of the used amorphous boron powder were: 96.7 wt.% B; ≤1.0 µm average particle size; very dark brown colour (as declared by manufacturer Sigma-Aldrich, St. Louis, Missouri, USA). The powder mixture (boron mixture) for the experiment was prepared by mixing amorphous boron powder with quartz sand (as diluent) in a mass ratio of 1:1 with the addition of 3 wt.% activator (NH<sub>4</sub>Cl). The prepared powder mixture and alumina samples were placed in a cylinder steel container with a cover (Ø64 mm × 50 mm × 5 mm) in the following order: ~5 mm quartz sand; ~5 mm boron mixture; alumina sample; ~5 mm boron mixture; ~5 mm quartz sand; ~15 mm clay to seal the container. After drying in an electrical furnace for 1 h at 105 ± 5 °C, the container was placed into the electrical furnace heated to the chosen experiment temperature (950 °C, 900 °C, 850 °C or 800 °C) for 2 h. After 2 h, container was pulled out of the furnace and left to cool at room temperature.

## 2.2. Thermal Spray Details

To evaluate the effect of boronizing on the alumina adhesion with nickel and nickel alloy, thermal spray experiments were conducted. Two types of spraying powder (from Oerlikon) were used: powder of self-fluxing reusable Ni-based alloy Metco 12C (nominal composition: 84.55% Ni, 7.5% Cr, 2.5% Fe, 0.25% C, 1.7% B, 3.5% Si; nominal particles size distribution:  $-75/+45\ \mu\text{m}$ ; melting point:  $<1100\ ^\circ\text{C}$ ) suitable for two-step spray-fuse process; that is, the coating was first deposited by thermal spray and then remelted by flame in the furnace or using other heating sources, along with the powder of pure nickel Metco 56C-NS (nominal composition: 99.3 wt.% Ni; nominal particles size distribution:  $-125/+53\ \mu\text{m}$ ; melting point:  $1455\ ^\circ\text{C}$ ). Metal powder was deposited on the reference and boronized alumina samples by oxy-fuel flame spraying using Rototec 80 (Castolin Eutectic) spraying equipment. The parameters of the spraying process were as follows: neutral flame;  $\sim 230\text{--}250\ ^\circ\text{C}$  substrate preheating temperature;  $\sim 150\ \text{mm}$  spraying distance;  $\sim 200\ \text{mm/s}$  spraying speed; the alumina substrates were coated by one spraying pass. Before spraying, the substrates were washed with isopropyl alcohol and dried with a hot air stream. The samples with deposited pure nickel were investigated in the as-spray state. Samples with deposited self-fluxing nickel alloy were then heated in the furnace for 180 s at  $1200\ ^\circ\text{C}$  to obtain partial melting of the deposited layer. Samples with adhered metal deposits were mounted in resin, cut across the interface, ground on diamond disc and polished with diamond suspensions for microscopic analysis.

## 2.3. Characterisation Methods

Scanning electron microscopy (SEM) was used for morphological study of the alumina surface after the boronizing and contact zone of the thermally sprayed alumina samples. The elemental composition of alumina surface areas, single crystals and cross sections was analysed by energy dispersive spectrometry (EDS). A scanning electron microscope SEM JEOL JSM-7600F (JEOL, Akishima, Japan) equipped with an energy dispersive spectrometer (EDS) Inca Energy 350 SDD X-Max  $20\ \text{mm}^2$  (Oxford Instruments, Oxford, UK) for X-ray microanalysis was used. SDD X-Max is a silicon drift detector (SDD) capable to analyse all elements from Be to Pu (including boron). The main SEM/EDS analysis parameters were: 10 kV accelerating voltage;  $\sim 8\ \text{mm}$  working distance; secondary electron signal for imaging. Before the analysis, the boronized alumina samples and prepared cross sections of thermally sprayed samples were coated with gold film to provide electric conductivity.

The analysis of phase composition of the boronized alumina surfaces was performed by the X-ray diffraction (XRD) method using a DRON-7 diffractometer (St. Petersburg, Russia) at 30 kV voltage and 12 mA current, with a Cu-K $\alpha$  ( $\lambda_m = 0.154178\ \text{nm}$ ) radiation, a 2-Theta angle range from  $4^\circ$  to  $80^\circ$ , a scanning step of  $0.02^\circ$  and a per-step duration of the intensity measurement of 2 s. The phases were identified by decoding the XRD patterns according to the ICDD diffraction database.

XPS characterization of the alumina surfaces was carried out using the Kratos AXIS Supra+ spectrometer (Shimadzu Corporation, Kyoto, Japan) with monochromatic Al K $\alpha$  (1486.6 eV) X-ray radiation powered at 225 W. The base pressure in the analysis chamber was less than  $1 \times 10^{-8}$  mbar, and a low electron flood gun was used as charge neutralizer. The survey spectra for each sample were recorded at a pass energy of 40 eV in 0.5 eV step and high-resolution spectra (pass energy 10 eV, in 0.1 eV steps) over individual element peaks. The binding energy scale was calibrated by setting the C1s hydrocarbon peak at 284.8 eV. For sputter experiments, the monoatomic Ar $^+$  ion gun (Minibeam 6) with an energy of 5 keV and  $110\ \mu\text{m}$  aperture was used. The effective sputtering rates were 3.2 nm/min measured at a SiO $_2$  reference sample. After sputtering for 1200 s, the high-resolution scan spectrum for each element was obtained, and the chemical composition was determined from corresponding XPS peak areas after inelastic background subtraction and using the relative sensitivity.

### 3. Results

#### 3.1. Characterisation of the Alumina Surface by SEM, EDS, XPS and XRD Methods

Figure 1 shows the surface morphology of the  $\text{Al}_2\text{O}_3$  samples before (Figure 1a) and after boronizing at different temperatures (Figure 1b–i). The surface of the reference sample (R) had a microstructure of irregular-shaped grains with sizes up to  $\sim 10\ \mu\text{m}$  (Figure 1a). After thermochemical treatment for 2 h at  $800\ ^\circ\text{C}$ , the single discrete centres of the formation of the new phase on the surface were observed (Figure 1b). X-ray microanalysis by EDS technique showed the presence of  $\sim 9\ \text{wt.}\%$  B (or  $\sim 15\ \text{at.}\%$ ). Taking into account poor EDS sensitivity to light elements, lower real boron concentration may be assumed. As can be seen from Figure 1c, the new phase crystallized in the needle-shaped crystals. According to EDS, the crystals formed consisted mainly of oxygen ( $\sim 65\ \text{at.}\%$ ), boron ( $\sim 17.5\ \text{at.}\%$ ) and aluminium ( $\sim 15\ \text{at.}\%$ ); Ca, Si and Mg made up the remaining few percent. Taking into account obtained elemental composition and morphology of the appeared crystals, the formation of some type of aluminium borate may be assumed, which is well consistent with the results presented in [14]. Hernández et al. [14] showed in their study that the formation of aluminium borates ( $\text{Al}_{18}\text{B}_4\text{O}_{33}$  and  $\text{Al}_4\text{B}_2\text{O}_9$ ) from alumina and boron oxide occurs at  $800\ ^\circ\text{C}$ . In addition to the formed needle-shaped crystals, signs of the formation of new crystals were observed on the faces of alumina grains (Figure 1d). However, this phenomenon was only occasional. With the increase of the boronizing temperature up to  $850\ ^\circ\text{C}$ , the average boron concentration at the surface slightly increased (up to  $\sim 12\ \text{wt.}\%$  or  $\sim 19\ \text{at.}\%$ ), and the amount of the formed needle-like crystals and the length of the individual needles visibly increased (Figure 1e). The thickness of the formed needle grains was between  $\sim 0.2$  and  $\sim 1.0\ \mu\text{m}$ , and the aspect ratio was between  $\sim 20:1$  and  $\sim 15:1$  (Figure 1f). The elemental composition of the formed crystals was similar to that obtained at  $800\ ^\circ\text{C}$ . The slight variation of elements concentrations may be related to the peculiarities of the EDS method and the possible non-uniform distribution of elements within the individual crystal. It can also be noted that several crystals grew from one crystallization centre, where the presence of some particles can be observed, most likely amorphous boron. Respectively, one may assume that in this case, the crystallisation occurred in the points where the amorphous boron particles had good physical contact with the alumina surface, providing the possibility of a chemical interaction and resulting in the appearance of the new phase. However, a major part of the surface remained unmodified. After boronizing at  $900\ ^\circ\text{C}$ , boron concentration at the surface increased up to  $\sim 21.5\ \text{at.}\%$ , and almost the entire surface was covered with crystals of the new phase (Figure 1g). Two distinct surface zones of crystals were observed, which are marked in Figure 1g as “1” and “2”. In zone “1”, coarser needle-like crystals growing mainly in lateral surface direction and having a thickness up to  $\sim 3.2\ \mu\text{m}$  and aspect ratio up to  $\sim 20:1$  were observed. These zones were small islets ( $\sim 0.01\text{--}0.9\ \text{mm}^2$ ) and occupied  $\sim 10\%$  of the surface. The boron concentration in zones “1” was slightly higher ( $\sim 26.5\ \text{at.}\%$ ) than the average; this may be related with the presence of amorphous boron residues (Figure 1h). Zone “2” was characterised by the growth of much finer crystals—nano-rods of  $\sim 100\text{--}150\ \text{nm}$  thickness and  $\sim 1\text{--}2\ \mu\text{m}$  length. The presented SEM images clearly reveal that nano-rods crystallized from the  $\text{Al}_2\text{O}_3$  grain faces and grew near perpendicular to them (Figure 1i); that is, the nano-rods orientation in the formed aluminium borate layer depended on the primary orientation of the  $\text{Al}_2\text{O}_3$  grains at the sample surface. The morphology of the nano-rods formed was very similar to that of the nano-rods obtained by Hernández et al. [14] at  $1100\ ^\circ\text{C}$ . At the same time, no residues of the amorphous boron powder or other particles were observed on the surface of  $\text{Al}_2\text{O}_3$ , indicating that the growth of nano-rods was a result of atomic boron diffusion into the surface and the change of elemental surface composition. With the further temperature increase up to  $950\ ^\circ\text{C}$ , the average boron concentration at surface increased up to  $\sim 24.5\ \text{at.}\%$  (by EDS), and the entire surface was covered with aluminium borate nano-rods layer (Figure 1j,k). However, occasional surface islets, where needle-like crystals were distributed in a visually glassy layer with the increased silicon concentration, were observed (Figure 1l), indicating that at the temperature of  $950\ ^\circ\text{C}$  quartz used in the mixture with amorphous

boron reacted with alumina and boron with the formation of some phases, possibly having a glassy nature.

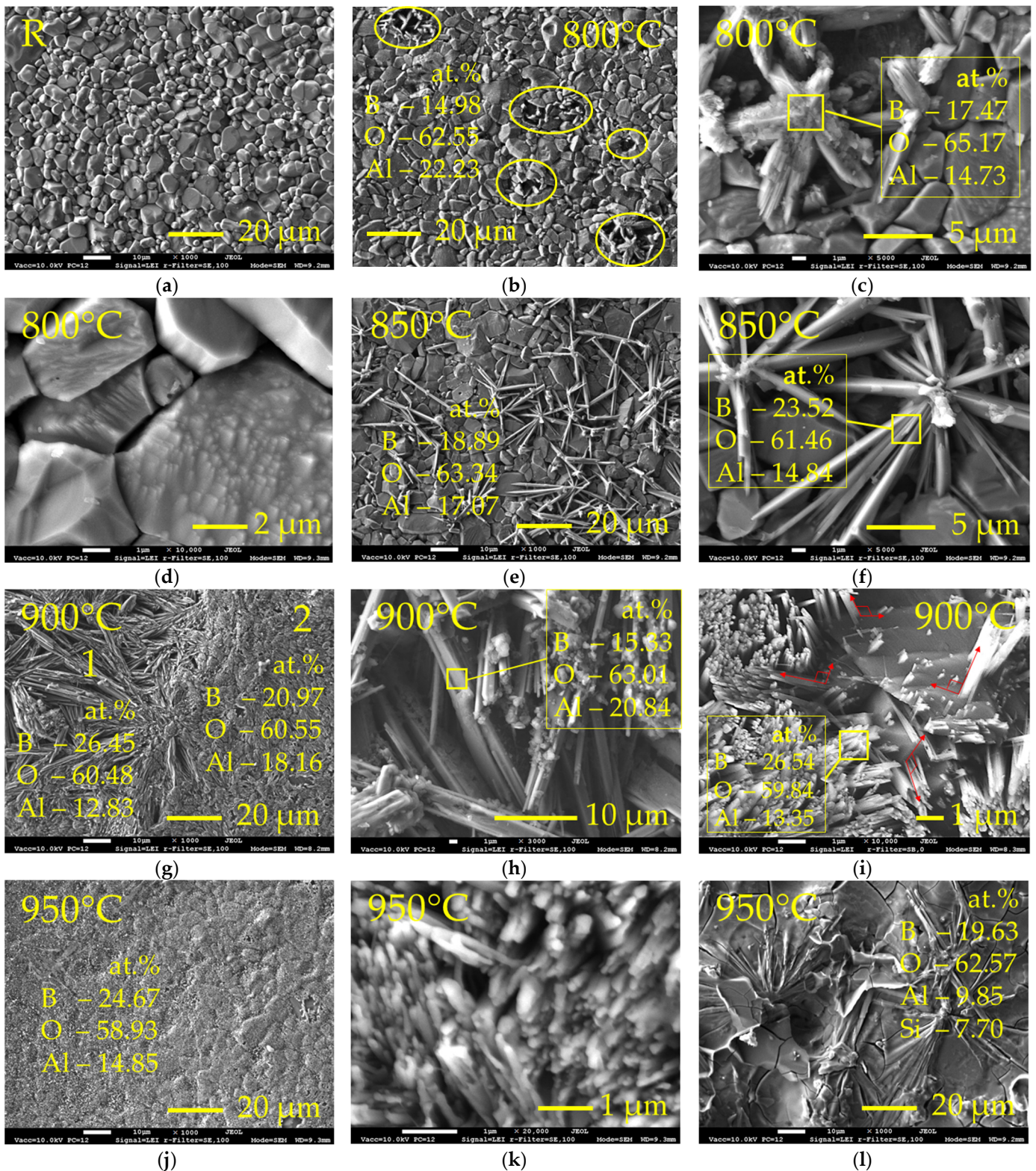


**Figure 1.** SEM micrographs of the reference  $\text{Al}_2\text{O}_3$  sample surface (a) and surfaces of  $\text{Al}_2\text{O}_3$  samples after boronizing at 800 °C (b–d), 850 °C (e,f), 900 °C (g–i) and 950 °C (j–l) temperatures; (b) yellow ovals show points of the appearance of aluminium borate crystals on surface; in images, the concentration of major elements is given (the remaining are Ca, Mg, Si); R—reference sample.

According to the results of the X-ray diffraction analysis, the control samples consisted mainly of  $\alpha$ - $\text{Al}_2\text{O}_3$ ; the minor reflections attributable to  $\theta$ - $\text{Al}_2\text{O}_3$  were identified in the diffraction curve as well (Figure 2, “R”). The results of the SEM and EDS analyses allowed us to assume the formation of aluminium borates—compounds typical for the  $\text{Al}_2\text{O}_3$ – $\text{B}_2\text{O}_3$  system. Gielisse and Foster [15] obtained two stable borates in this binary system— $\text{Al}_4\text{B}_2\text{O}_9$  and  $\text{Al}_{18}\text{B}_4\text{O}_{33}$ . Hernández et al. [14] indicated that  $\text{Al}_4\text{B}_2\text{O}_9$  and  $\text{Al}_{18}\text{B}_4\text{O}_{33}$  formation from alumina and boron oxide occurs between 600 and 800 °C. Since the temperature of boronizing was between 800 and 950 °C, either could be obtained in the present experiments. The surface on the samples boronized at 800 °C and 850 °C contained very few crystals for the new phase. Therefore, the X-ray diffraction signal from these surfaces was too low. The layer thickness of the new crystals formed after boronizing at 900 °C and 950 °C was between one and a few micrometres, which is much lower than the depth of X-ray diffraction analysis. Therefore, major reflections attributable to  $\alpha$ - $\text{Al}_2\text{O}_3$  and  $\theta$ - $\text{Al}_2\text{O}_3$  were observed on the diffraction curves of boronized samples, the same as the reference. In addition, the XRD patterns of boronized samples revealed the presence of reflections at 2-Theta angle  $\sim 16.5^\circ$ ,  $\sim 26.4^\circ$  and  $\sim 33.3^\circ$  (Figure 2, “950 °C”), which may be assigned either to  $\text{Al}_4\text{B}_2\text{O}_9$  or  $\text{Al}_{18}\text{B}_4\text{O}_{33}$ . However, the absence of any evidence of peak formation at 2-Theta angle  $\sim 20.4^\circ$  (typical for  $\text{Al}_{18}\text{B}_4\text{O}_{33}$ ) indicates that aluminium borate of the  $\text{Al}_4\text{B}_2\text{O}_9$  type rather than  $\text{Al}_{18}\text{B}_4\text{O}_{33}$  may be assumed in this case.

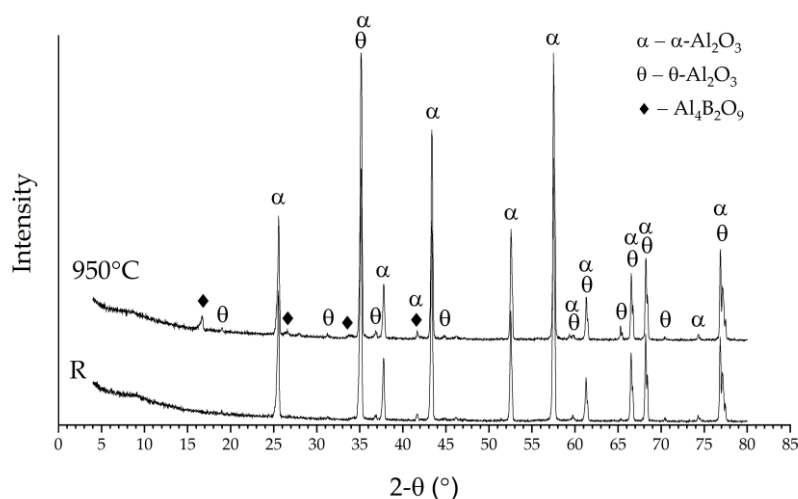


**Figure 2.** XRD patterns of the reference sample (R) and sample boronized at 950 °C.

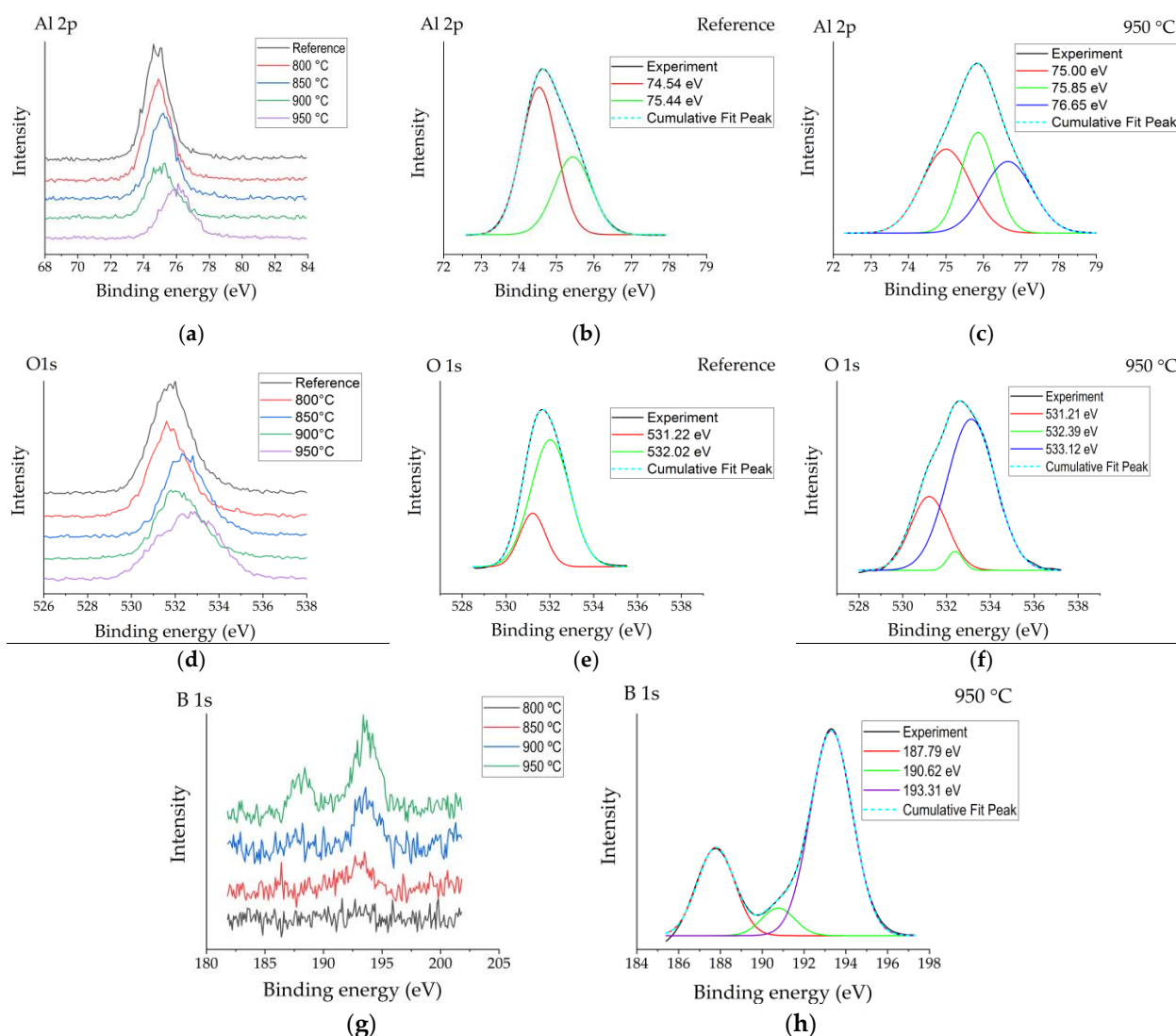
Average boron concentrations determined in modified  $\text{Al}_2\text{O}_3$  surfaces by EDS method were between  $\sim 15$  and  $\sim 25$  at.% and showed an expressed dependence on the process temperature. Taking into account the peculiarities of the EDS technique, the lower real concentrations may be assumed. The elemental composition of the modified surfaces was also analysed by the XPS method (Table 1). The results revealed the presence of boron in a range between 2.6 and 15.21 atomic percent, which is much lower as compared with EDS results. Although the surfaces were etched for 1200 s prior to the spectra recording, XPS analysis showed the presence of significant concentrations of carbon, which appeared here most likely due to  $\text{CO}_2$  adsorption. This led to some distortion in the ratio of the main elements in the results. Moreover, the carbon concentration was higher in processed samples as compared with the reference, which may be related to the more developed surface morphology and increased true surface area that appeared with the formation of aluminium borate crystals, which resulted in more significant  $\text{CO}_2$  adsorption.

Figure 3 shows the  $\text{Al}2p$ ,  $\text{O}1s$  and  $\text{B}1s$  peaks obtained by X-ray photoelectron spectroscopy for the reference sample and samples boronized at different temperatures. Figure 3a reveals an  $\text{Al}2p$  peak centred at  $\sim 74.8$  eV for the reference sample. The position of the  $\text{Al}2p$  peak for the sample boronized at 800 °C did not differ visibly from that of the reference, while with further temperature increases, a slight peak position shift to the higher

binding energies was observed. For the reference sample, two peaks with binding energies of ~74.5 eV and 75.4 eV were deconvoluted (Figure 3b), which, according to various sources [16,17], are typically attributed to  $\text{Al}_2\text{O}_3$  and surface-bound hydroxyl groups on Al (Al–OH). For boronized surfaces, the appearance of one more peak component was observed at a higher binding energy (~76.65 eV), which was most expressed for samples boronized at higher temperatures containing more boron and showing plenty crystallization of aluminium borate crystals (Figure 3c). In borates, boron and oxygen atoms form planar trigonal  $\text{BO}_3$  units or negatively charged tetrahedral  $[\text{BO}_4]^-$  units based on strong covalent boron–oxygen bonds [18]. Respectively, the appearance of this peak might be attributed to borate units bound to aluminium (Al–O–B).

**Table 1.** Elemental composition of  $\text{Al}_2\text{O}_3$  samples' surface (in at.%, by XPS).

Sample	B	Al	Si	C	O	K
Reference	-	33.86	3.26	5.43	57.45	-
800 °C	2.60	31.88	1.88	9.0	55.33	-
850 °C	4.64	20.86	6.01	17.75	49.47	1.21
900 °C	12.20	20.90	1.78	13.10	50.62	1.39
950 °C	15.21	16.43	1.30	16.48	49.64	0.92



**Figure 3.** XPS spectra patterns of the reference sample (R) and boronized samples: (a) high-resolution

Al2p spectra measured for the reference and boronized samples; (b,c) deconvoluted Al2p spectra for reference sample and sample boronized at 950 °C, respectively; (d) high-resolution O1s spectra measured for the reference and boronized samples; (e,f) deconvoluted O1s spectra for reference sample and sample boronized at 950 °C, respectively; (g) high-resolution B1s spectra measured for the reference and boronized samples; (h) deconvoluted O1s spectra for sample boronized at 950 °C.

In their study, Ogugua et al. [19] investigated an iron-doped  $\text{ZnAl}_2\text{O}_4$  system and determined Al2p peak's shift to higher binding energies with the increase of iron concentration. The authors assigned the appearance of Al2p peak components at 76.0 eV and 76.1 eV to Al–O–Fe. The authors related the appearance of the peak assigned to Al–O–Fe at a higher binding energy than that of peaks assigned to Al–O and Al–OH with higher electronegativity of Fe (1.83) than Al (1.61). Taking into account that the electronegativity of boron is even higher (2.0), the appearance of the Al–O–B peak component at higher binding energies looks to be reasonable. O1s peaks of boronized surfaces were also shifted to higher binding energies as compared with the reference (Figure 3d). For the non-modified  $\text{Al}_2\text{O}_3$  surface, two peaks' components were observed after deconvolution (Figure 3e)—the peak at ~531.2 eV ascribed to O in  $\text{Al}_2\text{O}_3$  and the peak at ~532.0 eV typically assigned to  $\text{OH}^-$ , chemisorbed oxygen or dissociated oxygen [17]. For boronized samples, one more peak at higher binding energy ~533.1 eV appeared (Figure 3f), which, according to [20], may be attributed to O–B bonds. The results of the analysis of B1s peaks were consistent with the studies presented above and confirmed them in general. All B1s spectra obtained have shown peaks centred at ~193.3 eV (Figure 3g), attributable to B–O [20]. For more intensive spectra obtained at surfaces boronized at 900–950 °C, a peak centred at ~187.8 eV was observed, as well as a minor peak at ~190.6 eV (Figure 3h), which, based on the results reported earlier [19], may be assigned to B–O–Al bonds. The peak at 187.8 eV here should most likely be attributed to elemental boron from amorphous boron residues on the surface.

### 3.2. Adhesion of Ni-Based

To evaluate the possibility to improve the adhesion between the alumina ceramic and metal melt by the thermochemical boronizing, pure nickel and self-fluxing refusable Ni-based alloy Metco 12C were thermally sprayed onto the surface of reference alumina sample, and the samples were boronized at different temperatures.

As expected, neither a pure nickel layer nor nickel alloy layer were formed onto the reference surface. After deposition and cooling in air, the layers detached. Samples boronized at 800 °C, 850 °C and 900 °C did not show an improvement in metal adhesion to alumina. As a result of boronizing, aluminium borate formed on the surface, known as a quite inert material. Therefore, such result of the metal deposition experiment was predictable as well. However, the metal layers and individual splats adhered to the surface of samples boronized at 950 °C. Figure 4 shows the SEM micrographs of the samples cross sections prepared after thermal spray (for pure nickel) and subsequent heating at 1200 °C (for self-fluxing alloy). The shape of the individual splat shown in Figure 4a allows an approximate estimate of the contact angle and shows that the well wetting of the alumina surface was not achieved. However, as may be seen from Figure 4a–e, some intermediate layer was formed between the metal splat/layer and ceramic substrate, providing adhesion between them. The observation of the interface at a higher magnification (Figure 4f) shows that after spraying and heating, a solid layer formed at the alumina surface, in which the borate nano-rods were not present as individuals but were incorporated in a solid matrix. Between this layer and metal deposit, the intermediate layer may be observed, which provides adhesion between the ceramic substrate and Ni-based alloy deposit.

According to the EDS analysis, the intermediate layer formed consisted mainly of boron, oxygen and aluminium; the presence of some silicon was established as well (Table 2). Respectively, the formation of  $\text{Al}_2\text{O}_3$ – $\text{B}_2\text{O}_3$ – $\text{SiO}_2$  glass may be assumed here, and the participation of the silicon in the formation of bond layer should be pointed out. According to [14],  $\text{Al}_4\text{B}_2\text{O}_9$  is stable up to 1100 °C. Wang et al. [21] showed that during thermal analysis

at a temperature of 1150 °C,  $\text{Al}_4\text{B}_2\text{O}_9$  melts and yields  $\text{Al}_{18}\text{B}_4\text{O}_{33}$  with slowly evaporating  $\text{B}_2\text{O}_3$ . Thus, one may assume that here,  $\text{B}_2\text{O}_3$ , which formed at a high temperature due to the decomposition of  $\text{Al}_4\text{B}_2\text{O}_9$  during spraying and heating, reacted with  $\text{Al}_2\text{O}_3$  and silicon to form both an intermediate layer providing adhesion and solid nano-rods-containing layer at the alumina surface. In the case of self-fluxing Ni alloy, the source of silicon is the alloy itself. However, for pure nickel, the presence of silicon was established as well, indicating that here the enrichment of surface with silicon from the quartz sand used in the amorphous boron mixture as a diluent played an important role as well.

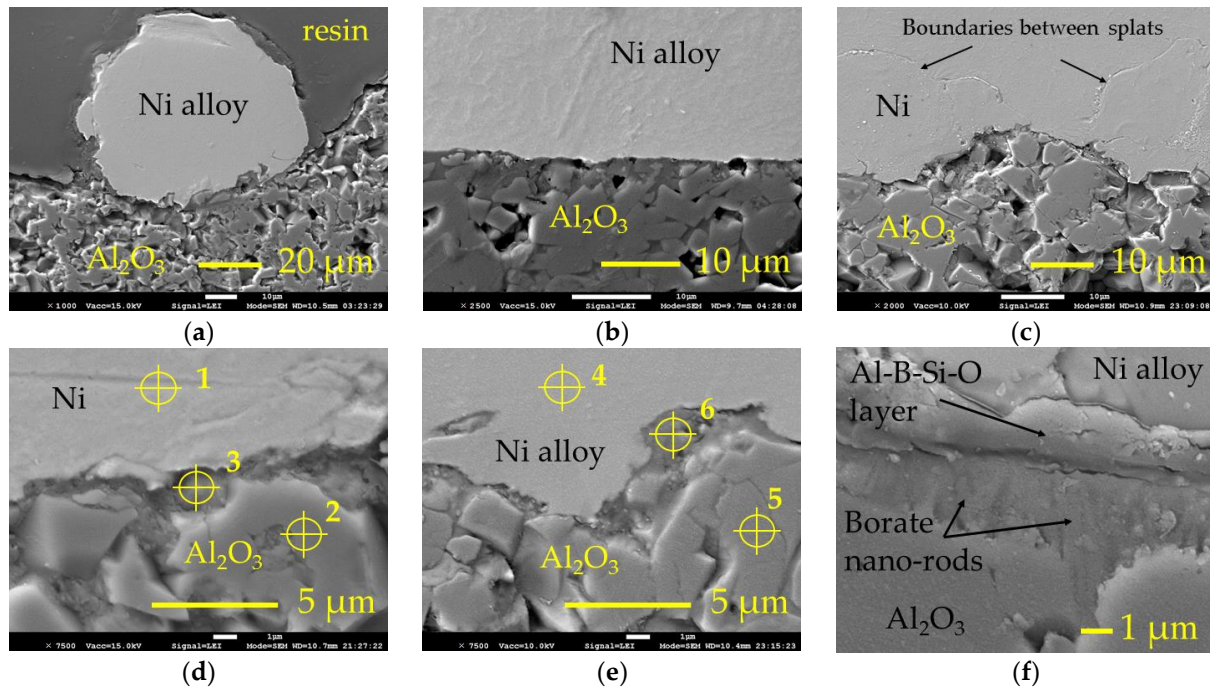


**Figure 4.** SEM micrographs of the thermally sprayed samples' cross sections: (a,b)—single splat and layer, respectively, of the self-fluxing Ni-based alloy on the surface of  $\text{Al}_2\text{O}_3$  boronized at 950 °C (after thermal spraying and post-heating at 1200 °C for 180 s); (c)—thermally sprayed layer of the pure nickel on the surface of  $\text{Al}_2\text{O}_3$  boronized at 950 °C; (d,e)—interface between the pure nickel and Ni-based alloy, respectively, deposit and ceramic substrate with marked points of EDS analysis; (f)—intermediate layer between Ni-based alloy deposit and borate layer; Ni—pure nickel; Ni alloy—self-fluxing re-fusible Ni-based NiCrFeCBSi alloy; 1–6—points of EDS analysis.

**Table 2.** Elemental composition of the metal deposits, ceramic substrate and interface areas marked in Figure 4 (in wt.%, by EDS).

Element	Metal Phase		Ceramic Phase		Intermediate Layer	
	1	4	2	5	3	6
B	-	1.8	10.9	1.7	38.7	24.8
O	2.8	1.7	50.4	51.6	26.3	44.0
Al	-	-	38.6	46.4	17.8	25.1
Si	-	2.6	0.1	-	3.7	4.9
K	-	-	-	-	0.3	0.2
Ca	-	-	-	0.2	-	0.9
Cr	-	5.8	-	-	-	-
Fe	-	6.6	-	-	-	-
Ni	97.2	81.6	-	-	13.3	-

#### 4. Discussion

The results of the SEM, EDS, XRD and XPS analyses revealed changes in the morphology along with elemental and phase compositions of  $\text{Al}_2\text{O}_3$  surface after boronizing at 800–950 °C. The formation of oxygen-containing Al–O–B compound crystallized in needle- or nano-rods shaped crystals was confirmed, which most likely may be identified as  $\text{Al}_4\text{B}_2\text{O}_9$  or  $\text{Al}_{18}\text{B}_4\text{O}_{33}$  aluminium borates. It was found that at lower boronizing temperatures, coarser needle-shaped crystals formed, most likely as a result of the  $\text{Al}_2\text{O}_3$  surface interaction with amorphous boron particles at the points of their good physical contact rather than as a result of boron atoms' diffusion into the surface. Pivkina et al. [22] showed in their study that the oxidation of amorphous boron particles begins at ~600 °C, which is much lower than the crystalline forms of boron. The authors related this phenomenon with the presence of some boron sub-oxide ( $\text{B}_6\text{O}$ ) on the surface of primary amorphous boron particles that makes them more chemically reactive at elevated temperatures. Jain et al. [23] indicated an even lower temperature of boron powder oxidation start (700 K). Therefore, it is possible that the oxidation of boron first takes place (at the presence of residual air in hermetic container), and then nucleation and growth of aluminium borate crystals occurs by the reaction  $9\text{Al}_2\text{O}_{3(s)} + 2\text{B}_2\text{O}_{3(L)} \rightarrow \text{Al}_{18}\text{B}_4\text{O}_{33(s)}$  [2], or, by analogy,  $2\text{Al}_2\text{O}_{3(s)} + \text{B}_2\text{O}_{3(L)} \rightarrow \text{Al}_4\text{B}_2\text{O}_{9(s)}$ . Boronizing at 900 °C and 950 °C resulted in significant crystallisation of nano-rod-like shaped aluminium borate growing from the faces of the alumina grains as a result of the alumina surface enrichment with boron, which was due to thermochemical treatment as such. The characterisation methods applied in the present study did not allow us to unambiguously identify the type of the borates formed. However, EDS showed a slightly higher concentration of boron for nano-rods-shaped crystals obtained as a result of thermo-chemical enrichment. Possibly, the formation of two types of aluminium borates takes place here—coarser needle-shaped  $\text{Al}_{18}\text{B}_4\text{O}_{33}$  and  $\text{Al}_4\text{B}_2\text{O}_9$  nano-rods. However, further investigation is required for more precise identification of the formed compounds.

The present investigation was initiated to evaluate the possibility to modify the alumina wettability by metal melts using thermochemical treatment. The results revealed that significant improvement of wetting by pure nickel or nickel alloy did not occur on the boronized alumina surface. However, it should be noted that the conditions of the melting experiment conducted in the present study were close to the real conditions of the production of thermally sprayed coatings and differed from those of wetting experiments presented in the works mentioned above. It is widely reported that the oxidation medium influences the contact angle and, most likely, better wetting would have been obtained in the present study in a vacuum or inert melting medium. The technology of boronizing in the amorphous boron medium used in this study can hardly be considered as an effective method to improve the wettability of the alumina surface with nickel melts. However, some improvement of adhesion between the nickel/nickel alloy and  $\text{Al}_2\text{O}_3$  surface was obtained due to the formation of a glassy phase consisting of B, O, Al and Si between the metal and ceramic surfaces at the presence of some silicon at the modified surfaces.

Aluminium borates are known as main stable phases in the  $\text{Al}_2\text{O}_3$ – $\text{B}_2\text{O}_3$  binary system [14,24]. Materials based in these phases possess a number of valuable properties such as a low density and thermal expansion coefficient, good mechanical properties, high refractoriness, chemical inertness and resistance to acids and alkalis, including hot mineral acids and borate glasses' melts, that makes them prospective in various fields [14,24]. Aluminium borates may be considered as the aggregate for heat-resistant rubber, cements, ceramics and other composite materials. The obvious practical and scientific importance of aluminium borates are related to the significant catalytic activeness of these materials [25,26]. A characteristic feature of aluminium borates is the ability to form needle-like crystals. Currently, the use of needles/whiskers of aluminium borate for strengthening alloys comes to the fore [27]. Due to the ability of needle-like crystals to pierce cells' walls, aluminium borate is used in genetic engineering [28]. Recently, there has been a growing interest in these materials and new simple methods to synthesize them. A number of

methods have been suggested to synthesize aluminium borate powder or obtain compact ceramic. The review of the methods is available in [24]. The presented experimental study demonstrates that thermochemical boronizing of alumina in amorphous boron solid medium is a simple method to obtain a thin aluminium borate layer consisting of oriented nano-rod-like crystals, whose growing direction is predetermined by the orientation of alumina grains' faces at surface.

## 5. Conclusions

The following general conclusions were drawn from the results of experimental research described in this paper:

1. The application of thermochemical boronizing in a solid medium of amorphous boron at the temperatures of 900–950 °C resulted in an enrichment of the alumina surface with boron and the formation of oxygen-containing compounds typical for the  $\text{Al}_2\text{O}_3$ – $\text{B}_2\text{O}_3$  system—borates.
2. Thermochemical boronizing of alumina in amorphous boron medium at 900–950 °C temperatures allowed us to obtain the aluminium borate layer of the oriented nano-rod-like crystals, whose growing direction is largely predetermined by the orientation of the alumina grains' faces at surface.
3. The adhesion between nickel or self-fluxing nickel alloy and the boronized alumina surface was obtainable due to the formation of an intermediate layer consisting of B, O, Al and Si between the metal and ceramic surfaces at the presence of some silicon at the modified alumina surface.

**Author Contributions:** Conceptualization, J.Š. and O.Č.; methodology, J.Š. and O.Č.; formal analysis, A.L.; investigation, J.Š., A.L., O.Č. and R.S.; resources, R.S.; writing—original draft preparation, J.Š. and A.L.; writing—review and editing, O.Č. and R.S.; supervision, J.Š. All authors have read and agreed to the published version of the manuscript.

**Funding:** This research received no external funding.

**Institutional Review Board Statement:** Not applicable.

**Informed Consent Statement:** Not applicable.

**Data Availability Statement:** Not applicable.

**Conflicts of Interest:** The authors declare no conflict of interest.

## References

1. Walker, C.A. 16-Metal–nonmetal brazing for electrical, packaging and structural applications. In *The Series Welding and Other Joining Technologies, Advances in Brazing*; Sekulić D., P., Ed.; Woodhead Publishing: Sawston, UK, 2013; pp. 498–524. [\[CrossRef\]](#)
2. Michalak, M.; Latka, L.; Sokolowski, P.; Toma, F.-L.; Myalska, H.; Denoirjean, A.; Ageorges, H. Microstructural, mechanical and tribological properties of finely grained  $\text{Al}_2\text{O}_3$  coatings obtained by SPS and S-HVOF methods. *Surf. Coat. Technol.* **2020**, *404*, 126463. [\[CrossRef\]](#)
3. Bolelli, G.; Colella, A.; Lusvarghi, A.L.; Puddu, P.; Rigon, R.; Sassatelli, P.; Testa, V. Properties of HVOF-sprayed TiC-FeCrAl coatings. *Wear* **2019**, *418–419*, 36–51. [\[CrossRef\]](#)
4. Testa, V.; Morelli, S.; Bolelli, G.; Benedetti, B.; Puddu, P.; Sassatelli, P.; Lusvarghi, L. Alternative metallic matrices for WC-based HVOF coatings. *Surf. Coat. Technol.* **2020**, *402*, 126308. [\[CrossRef\]](#)
5. Song, B.; Murray, J.W.; Wellman, R.G.; Pala, Z.; Hussain, T. Dry sliding wear behaviour of HVOF thermal sprayed WC-Co-Cr and WC-Cr<sub>x</sub>C<sub>y</sub>-Ni coatings. *Wear* **2020**, *442–443*, 203114. [\[CrossRef\]](#)
6. Chirambaram, P.R.; Edwards, G.R.; Olsan, D.L. A thermodynamic criterion to predict wettability at metal-alumina interface. *Metall. Trans. B* **1992**, *23B*, 215–222. [\[CrossRef\]](#)
7. Naidich, Y. The wettability of solids by liquid metals. *Prog. Surf. Membr. Sci.* **1981**, *14*, 353–486.
8. Nogi, K.; Iwamoto, N.; Ogino, K. Wetting phenomena at high temperature (Part II). *Trans. JWRI* **1992**, *21*, 141–148.
9. Nakashima, K.; Takihira, K.; Mori, K.; Shinozaki, N. Wettability of  $\text{Al}_2\text{O}_3$  substrate by liquid iron—Effects of oxygen in liquid iron and purity of  $\text{Al}_2\text{O}_3$  substrate. *Mater. Trans. JIM* **1992**, *33*, 918–926. [\[CrossRef\]](#)
10. Harding, F.L.; Rossington, D.R. Wetting of ceramic oxides by molten metals under ultrahigh vacuum. *J. Am. Ceram. Soc.* **1970**, *53*, 87. [\[CrossRef\]](#)

11. Valenza, F.; Muolo, M.L.; Passerone, A. Wetting and interactions of Ni- and Co-based superalloys with different ceramic materials. *J. Mater. Sci.* **2010**, *45*, 2071–2079. [[CrossRef](#)]
12. Sousa, J.M.S.; Pereira, F.R.M.; Castro, R.M.; Curi, E.I.M. Abrasion resistance of Ni-Cr-B-Si coating deposited by laser cladding process. *Tribol. Int.* **2020**, *143*, 106002. [[CrossRef](#)]
13. Kulka, M. *Current Trends in Boriding: Techniques*; Springer: Chambersburg, PA, USA, 2019; p. 293.
14. Hernández, M.F.; Suárez, G.; Cipollone, M.; Conconi, M.S.; Aglietti, E.F.; Rendtorff, N.M. Formation, microstructure and properties of aluminum borate ceramics obtained from alumina and boric acid. *Ceram. Int.* **2017**, *43*, 2188–2195. [[CrossRef](#)]
15. Gielisse, P.J.M.; Foster, W.R. The System  $\text{Al}_2\text{O}_3\text{--B}_2\text{O}_3$ . *Nature* **1962**, *195*, 69–70. [[CrossRef](#)]
16. Usman, M.; Arshad, M.; Suvanam, S.S.; Hallén, A. Influence of annealing environment on the ALD- $\text{Al}_2\text{O}_3$ /4H-SiC interface studied through XPS. *J. Phys. D Appl. Phys.* **2018**, *51*, 105111. [[CrossRef](#)]
17. Celebioglu, A.; Vempati, S.; Ozgit-Akgun, C.; Biyikliab, N.; Uyar, T. Water-soluble non-polymeric electrospun cyclodextrin nanofiber template for the synthesis of metal oxide tubes by atomic layer deposition. *RSC Adv.* **2014**, *4*, 61698–61705. [[CrossRef](#)]
18. Cahit, H. Borates. In *Encyclopedia of Geology*, 2nd ed.; Alderton, D., Elias, S.A., Eds.; Academic Press: New York, NY, USA, 2021; Volume 1, pp. 489–504. [[CrossRef](#)]
19. Ogugua, S.; Ntwaeaborwa, O.; Swart, H. Luminescence structure and insight on the inversion degree from normal to inverse spinel in a  $\text{ZnAl}_{(2-x)}\text{Fe}_x^{3+}\text{O}_4$  system. *Bol. Soc. Esp. Ceram.* **2021**, *60*, 147–162. [[CrossRef](#)]
20. Ghadimi, Z.; Esfahani, H.; Mazaheri, Y. Control on nanostructured quaternary Ti-Al-O-B composite synthesized via electrospinning method, from nanoparticles to nanowhiskers. *J. Sol-Gel Sci. Technol.* **2021**, *98*, 127–137. [[CrossRef](#)]
21. Wang, J.; Ning, G.; Yang, X.; Gan, Z.; Liu, H.; Lin, Y. Large-scale synthesis of  $\text{Al}_4\text{B}_2\text{O}_9$ / $\text{Al}_{18}\text{B}_4\text{O}_{33}$  whiskers via a novel method. *Mater. Lett.* **2008**, *62*, 1208–1211. [[CrossRef](#)]
22. Pivkina, A.N.; Muravyev, N.V.; Monogarov, K.A.; Meerov, D.B.; Fomenkov, I.V.; Skryleva, E.A.; Milekhin, Y.M. Comparative analysis of boron powders obtained by various methods. I. Microstructure and oxidation parameters during heating. *Combust. Expl. Shock Waves* **2018**, *54*, 450–460. [[CrossRef](#)]
23. Jain, A.; Joseph, K.; Anthonysamy, S.; Gupta, G.S. Kinetics of oxidation of boron powder. *Thermochim. Acta* **2011**, *514*, 67–73. [[CrossRef](#)]
24. Yarotskaya, E.G.; Fedorov, P.P. Aluminum borate and methods of its synthesis overview. *Condens. Matter Interphases* **2018**, *20*, 348–353. [[CrossRef](#)]
25. Peil, K.P.; Galya, L.G.; Marcelin, G. Acid and catalytic properties of nonstoichiometric aluminum borates. *J. Catal.* **1989**, *115*, 441–451. [[CrossRef](#)]
26. MacKenzie, K.; Smith, M.; Kemp, T.; Voll, D. Crystalline aluminium borates with the mullite structure: A  $11\text{B}$  and  $27\text{Al}$ . Solid-state NMR Study. *Appl. Magn. Reson.* **2007**, *32*, 647–662. [[CrossRef](#)]
27. Chang, Z.; Lan, Q.; Wu, Y.; Su, N.; Deng, Q.; Ding, C.; Iizuka, T.; Peng, L.; Ding, W. Interfacial reaction of aluminum borate whisker reinforced Mg-10Gd-3Y-1Zn-0.4Zr (wt%) alloy matrix composite. *Mater. Charact.* **2022**, *183*, 111649. [[CrossRef](#)]
28. Mizuno, K.; Takahashi, W.; Beppu, T.; Shimada, T.; Tanaka, O. Aluminum borate whisker-mediated production of transgenic tobacco plants. *Plant. Cell Tissue Organ Cult.* **2005**, *80*, 163–169. [[CrossRef](#)]

**Disclaimer/Publisher's Note:** The statements, opinions and data contained in all publications are solely those of the individual author(s) and contributor(s) and not of MDPI and/or the editor(s). MDPI and/or the editor(s) disclaim responsibility for any injury to people or property resulting from any ideas, methods, instructions or products referred to in the content.